



HAL
open science

Single-Particle Model of Li-ion Battery – Model Calibration and Validation against Real Data in an Electric Vehicular Application

Iulian Munteanu, Antoneta Iuliana Bratcu, Pierre-Xavier Thivel, Yann Bultel, Didier Georges, Céline Decaux

► To cite this version:

Iulian Munteanu, Antoneta Iuliana Bratcu, Pierre-Xavier Thivel, Yann Bultel, Didier Georges, et al.. Single-Particle Model of Li-ion Battery – Model Calibration and Validation against Real Data in an Electric Vehicular Application. CPES 2024 - 12th IFAC Symposium on Control of Power & Energy Systems, International Federation of Automatic Control (IFAC), Jul 2024, Rabat, Morocco. hal-04580528

HAL Id: hal-04580528

<https://hal.science/hal-04580528>

Submitted on 1 Jun 2024

HAL is a multi-disciplinary open access archive for the deposit and dissemination of scientific research documents, whether they are published or not. The documents may come from teaching and research institutions in France or abroad, or from public or private research centers.

L'archive ouverte pluridisciplinaire **HAL**, est destinée au dépôt et à la diffusion de documents scientifiques de niveau recherche, publiés ou non, émanant des établissements d'enseignement et de recherche français ou étrangers, des laboratoires publics ou privés.

Single-Particle Model of Li-ion Battery – Model Calibration and Validation against Real Data in an Electric Vehicular Application ^{*}

Iulian Munteanu ^{*} Antoneta Iuliana Bratcu ^{*}
Pierre-Xavier Thivel ^{**} Yann Bultel ^{**} Didier Georges ^{*}
Céline Decaux ^{**}

^{*} Univ. Grenoble Alpes, CNRS, Grenoble INP^{*}, GIPSA-lab, 38000
Grenoble, France

^{*} Institute of Engineering and Management Univ. Grenoble Alpes
(e-mails:

{iulian.munteanu,antoneta.bratcu,didier.georges}@grenoble-inp.fr).

^{**} Univ. Grenoble Alpes, Univ. Savoie Mont Blanc, CNRS, Grenoble
INP^{*}, LEPMI, 38000 Grenoble, France

^{*} Institute of Engineering and Management Univ. Grenoble Alpes
(e-mails:

{pierre-xavier.thivel,yann.bultel,celine.decaux}@grenoble-inp.fr.

Abstract: This paper investigates the problem of calibration and validation of a battery electrochemical model as a mandatory step towards accurate estimation of battery important variables, like state of charge (SoC) and state of health (SoH). Here, the Single Particle Model (SPM) is considered, which mathematically describes the battery internal governing phenomena by means of parabolic partial differential equations (PDEs), but whose parameters are notoriously difficult to measure or estimate. After suitable approximation of this model through a linear finite-dimensional model, a systematic procedure of SPM calibration is here proposed and validated against real data issued from battery cycling in an electric vehicular application, *i.e.*, under standard driving cycle scenarios. In a novel approach of SoC estimation, the suitably calibrated SPM, together with measures of voltage and current, allow to analytically connect the internal spatially distributed ions' concentrations to the equilibrium concentration, which, at its turn, is an image of battery SoC. Results suggest that SPM can reliably predict the battery internal ions' concentrations and be further used for SoC accurate estimation.

Keywords: partial-differential-equation model, electrochemical model, Single Particle Model (SPM), model reduction, errors in variables identification, parameter identification.

1. INTRODUCTION

Use of Li-ion battery has been identified as the solution of choice in most electrical vehicle (EV) applications, due to its numerous advantages such as superior energy-to-weight ratio, high output current, deep discharge capability, large number of cycles, *etc.* However, optimal use of such battery is challenged by the need of battery states estimation throughout its useful life. Practical Li-ion cell state of charge (SoC) estimators, used in battery management systems, are notoriously approximative and with limited reliability. This is mainly due to the complexity of electrochemical phenomena, which renders difficult battery modeling and parameter estimation. The search for better SoC estimators is a richly investigated topic Di Domenico et al. (2010), Klein et al. (2012), Moura et al. (2016),

^{*} This work has been funded by IRGA ("Initiatives de Recherche à Grenoble Alpes") project PaDeSoH ("Partial-differential-equation-model-based estimation of battery state of health"), within the framework of "Investissement d'avenir" ANR-15-IDEX-02 French national research and innovation funding programme.

Zhang et al. (2020), sometimes relying upon physics-based electrochemical models Chaturvedi et al. (2010), more complex than the equivalent-electrical-circuit model.

The main drawback of these models is their complexity, which involves knowledge about many parameters, their accuracy being as good as parameters' values succeed in reflecting the cell real behavior. Hence, the interest of some practical guidelines for proper calibration of such models. This paper relies upon such battery modeling, developed from a dynamic-system, control-oriented perspective. Here, the Single Particle Model (SPM) is considered, which has been extensively approached in the literature – *e.g.*, Moura et al. (2012), Pozzato et al. (2021). Thus, an engineering-viewpoint methodology is here proposed, which is focused on practical aspects related to parameters identification and SPM calibration *vs.* a real cell operation, prior to its use for SoC estimation. This is not obvious, as the parameters are heavily dependent on the cell type, technology and manufacturer and parameter dispersion

is significant for Li-ion cells, which justifies that major research efforts have lately been dedicated to their identification – *e.g.*, Bizeray et al. (2018), Jin et al. (2018) and Li et al. (2020). In the same spirit, in this paper one strives to reduce the model complexity at a minimum, based on real data and engineering practice arguments, while retaining description of the phenomena essential for the cell electrochemical behavior.

This paper is organized as follows. Section 2 focuses on battery cell modeling, while Section 3 details the steps of SPM calibration based on a real cell behavior. Section 4 refers to model validation against real data and Section 5 concludes the paper.

2. SINGLE PARTICLE MODEL OF A LI-ION CELL

Basically, a battery cell is a sandwich comprising porous positive and negative electrodes and the electrolyte, the main behavior of charging/discharging being governed by intercalation (and deintercalation) of Li into the electrodes structure, as the cell is subjected to an electric current. It is widely agreed that this phenomenon, involving volumetric Li concentrations evolution within the electrodes volume, be modeled by a Fickian diffusion process, described by a set of parabolic partial differential equations (PDEs) for every elementary particle (or grain) in the electrode. The cell terminal voltage is a function of the Li concentrations in each electrode Chaturvedi et al. (2010). SPM (Fig. 1) has been developed as an efficient way to predict Li concentrations evolution and uses a single, equivalent spherical particle and a single PDE Santhanagopalan et al. (2006), Di Domenico et al. (2010). Next, for simplifying notations, we use subscripts “*p*” for positive electrode and “*n*” for the negative electrode.

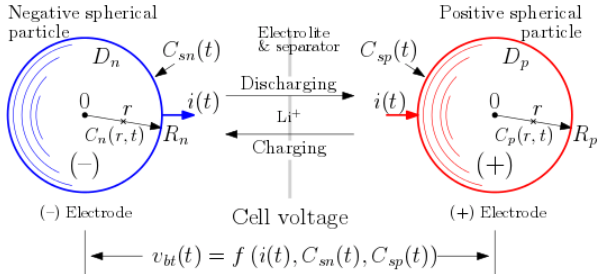


Fig. 1. SPM representation. The electrode is equivalent to a single porous spherical particle.

Lithium concentration within cell electrode is governed by a diffusion process, which, written in spherical coordinate, is expressed, *e.g.*, for positive electrode by:

$$\frac{\partial C_p}{\partial t}(r, t) = D_p \cdot \left[\frac{2}{r} \cdot \frac{\partial C_p}{\partial r}(r, t) + \frac{\partial^2 C_p}{\partial r^2}(r, t) \right], \quad (1)$$

where D_p is the diffusivity coefficient in the positive electrode and r is the space variable along the sphere radius (its radial coordinate). To this, Newman boundary conditions are added in the particle’s center and on its surface, respectively:

$$\begin{cases} \frac{\partial C_p}{\partial r}(0, t) = 0 \\ \frac{\partial C_p}{\partial r}(R_p, t) = \frac{i(t)}{D_p F a_p A L_p}, \end{cases} \quad (2)$$

with F being Faraday’s constant, R_p the positive particle radius, A the cell area, L_p the electrode thickness, a_p the specific interfacial surface area and $i(t)$ the cell current, whose sign convention is $i(t) > 0$ when charging and $i(t) < 0$ when discharging.

By solving these equations, one obtains the concentration on the particle surface, which has a special role, as it determines the cell voltage potential. This variable will be denoted by $C_{sn}(t)$ for the negative electrode and by $C_{sp}(t)$ for the positive electrode:

$$C_p(R_p, t) = C_{sp}(t). \quad (3)$$

Similar equations are written for expressing the negative electrode behavior, taking into account the inverse sense (sign) for the input current in the second equation of (2).

In EV applications, battery current is usually lower than 1C, when considering suitable vehicle autonomy. It is widely agreed that at these levels of current, Li concentration values remain practically constant in the electrolyte and mass transport effects within it are negligible. Hence, cell behavior can reasonably be given only by (1) and (2) expressed for both particles, which give Li concentrations in both electrodes. Also, experimental tests on cells submitted to EV-specific driving cycles – here, a current profile derived from the Worldwide Harmonized Light Vehicles Test Procedure (WLTP) WLTP3 (2023) was used – showed sufficiently small cell temperature variations (within $\pm 1.5^\circ\text{C}$), so that the temperature be considered constant within a discharge cycle.

Voltage of a cell depends on current and on Li concentration on particles’ surfaces and is given by the nonlinear equation (4) – see Butler-Volmer kinetics in Klein et al. (2012) and Moura et al. (2012)). Voltage dependence on current and particles’ surface concentrations is algebraic:

$$\begin{aligned} v_{bt}(t) = & \frac{RT}{\alpha_p F} \cdot \sinh^{-1} \left[\frac{i(t)}{2a_p A L_p i_0(C_{sp}(t))} \right] - \\ & - \frac{RT}{\alpha_n F} \cdot \sinh^{-1} \left[\frac{-i(t)}{2a_n A L_n i_0(C_{sn}(t))} \right] + R_f \cdot i(t) + \\ & + U_p(C_{sp}(t)) - U_n(C_{sn}(t)), \end{aligned} \quad (4)$$

with exchange current density, *e.g.*, in the positive particle:

$$i_{0p}(c_{sp}(t)) = k_p \cdot \sqrt{C_e^0 \cdot C_{sp}(t) [C_{maxp} - C_{sp}(t)]} \quad (5)$$

and parameters: α_p is the anodic transfer coefficient, k_p is the reaction rate and C_{maxp} is the maximum Li concentration in solid phase. Moreover, C_e^0 is the Li concentration in electrolyte phase, R_f is the lumped resistance, T is the cell temperature and R is the universal gas constant. The specific interfacial surface area writes as $a_p = 3\varepsilon_p/R_p$, where volume fraction ε_p is constant for a certain electrode.

A similar equation like (5) applies for the exchange current density in the negative particle, i_{0n} , which obviously depends on the negative particle parameters (α_n , k_n , *etc.*).

$U_p(C_{sp}(t))$ and $U_n(C_{sn}(t))$ are the so-called *equilibrium potentials*. They are material-dependent evolutions of actual normalized Li concentrations with respect to maximum ones, *i.e.*, the potential is a function of the amount of Li in the electrode (also called *degree of lithiation*) – see Figs. 2 a) and b). They are identified for each type of electrode material and are usually given in the concerned literature either as look-up tables or as an equation us-

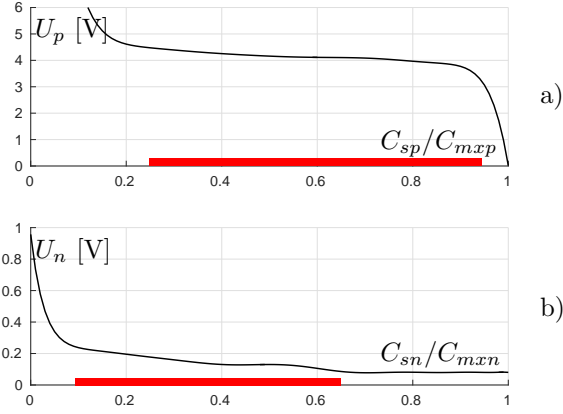


Fig. 2. Open-circuit potential as function of normalized concentration – Li et al. (2020): a) positive electrode, U_p ; b) negative electrode, U_n .

ing transcendental functions – see, for example, Li et al. (2020). Their difference gives the so-called cell open-circuit voltage: $V_{ocv}(t) = U_p(C_{sp}(t)) - U_n(C_{sn}(t))$.

The first two right-side terms of (4) denote cell overpotentials (of the positive and negative electrode, respectively), depending of both Li concentrations and the cell current. They are seen as an aggregated effect of a series resistance, which is variable with the Li concentrations on both particles' surfaces. The third term of (4) can be assimilated as an overpotential due to the lumped internal resistance, R_f . The sum of the first three terms in (4) is next referred to as the overvoltage, V_{ovm} :

$$V_{ovm}(t) = \frac{RT}{\alpha_p F} \cdot \sinh^{-1} \left[\frac{i(t)}{2a_p A L_p i_0(C_{sp}(t))} \right] - \frac{RT}{\alpha_n F} \cdot \sinh^{-1} \left[\frac{-i(t)}{2a_n A L_n i_0(C_{sn}(t))} \right] + R_f \cdot i(t). \quad (6)$$

The *state-space model* of Li concentrations is obtained by spatial derivative approximation *via* 1D discretization of spatial coordinate (*i.e.*, along the radius) within each spherical particle. Here, for a generic electrode/particle, for simplicity of writing, $C(r, t)$ represents the volumetric concentration within the sphere as function of the spatial coordinate, r , and time variable, t . Diffusion coefficient is noted by D and is considered constant.

For a mesh containing N nodes within the sphere, radius R is quantized in $(N + 1)$ domains having a quanta of $\Delta r = R/(N + 1)$. Note that this discretization defines $(N + 1)$ concentric spheres; Li volumetric concentrations $C_k(t)$ are defined within elementary volumes situated on the surface of each sphere having the index k . We note the time constant $\tau = \Delta r^2/D$ and the gain $G = DF a AL$.

Further, one uses the method of lines for approximating SPM PDE in (1) and explicit Euler's forward finite-difference method for the first spatial derivative approximation. However, in the second equation of (2) (*i.e.*, on the particle surface) backward differencing is used in derivative approximation, in order to remain within the physical range. The usual algebraic manipulations of these equations follow a similar approach as in Zhang et al. (2020) and lead to $(N + 2)$ equations describing the complete model of Li concentrations' evolution within the particle:

$$\begin{cases} \frac{dC_0(t)}{dt} = \frac{1}{\tau} [C_1(t) - C_0(t)] \\ \frac{dC_k(t)}{dt} = \frac{1}{k\tau} [(k+2)C_{k+1}(t) - 2(k+1)C_k(t) + kC_{k-1}(t)], \quad k = 1..N \\ \frac{dC_s(t)}{dt} = \frac{D}{G} \cdot \frac{N+3}{R} i(t) - \frac{1}{\tau} [C_N(t) - C_{N-1}(t)]. \end{cases} \quad (7)$$

The system state vector is composed of the Li concentrations in all spatial discretization points, including center of the generic spherical particle and its surface:

$\mathbf{x} \equiv \mathbf{C}_s = [C_0(t) \ C_1(t) \ C_2(t) \ \dots \ C_k(t) \ \dots \ C_N(t) \ C_s(t)]^T$. The input is the cell current, $u = i(t)$, and the output is the concentration of Li on the surface of the particle, $y = C_s(t) \equiv C_{N+1}(t)$. The ODEs describing Li diffusion within the particle under the influence of the cell current are thus described by (8), corresponding to a $(N+2)^{\text{th}}$ -order state space model (index \mathbf{P} comes from "particle"):

$$\begin{cases} \dot{\mathbf{x}}(t) = \mathbf{A}_P \cdot \mathbf{x}(t) + \mathbf{B}_P \cdot i(t) \\ C_s(t) = \mathbf{C}_P \cdot \mathbf{x}(t) \end{cases} \quad (8)$$

State-space matrices resulting from developing (7) for all discretization points k in the generic particle are given in (A.1) from Appendix A. Computation of \mathbf{A}_P eigenvalues yields a zero eigenvalue, which shows an integration effect within the Li concentration buildup, corresponding to the charging/discharging process (or otherwise cell SoC evolution). Also, the state matrix has a tri-diagonal structure and depends only on the time constant, τ , and on the number of spatial samples, N . The input matrix \mathbf{B}_P has a single non-zero element, denoted next as current gain, showing that the input variable, the current $i(t)$, acts directly only on the particle surface concentration, $C_s(t)$.

If letting $i(t) = 0$ in (8) – corresponding to what is called cell *relaxation* – an autonomous system is obtained, whose steady states are by definition the *equilibrium* Li concentrations, which depend on the initial concentrations just before zeroing the cell current. Therefore, the equilibrium concentrations – computed as the zero-input solution of (8) in response to initial concentrations – directly reflect the cell SoC, namely the one (just) before relaxation. Let us denote surface concentrations at cell equilibrium for SoC=0, C_{p0} and C_{n0} , and for SoC=1, C_{p1} and C_{n1} .

Let G_{in} and G_{ip} denote current gains for each of the two particles; *e.g.*, for the negative sphere, this gain writes as:

$$G_{in} = D_n(N+3)/(G_n R_n) = (N+3)/(3FA\varepsilon_n L_n). \quad (9)$$

Note that gains G_{ip} and G_{in} depend on the respective electrode geometry – surface, thickness and volume fraction – and they have opposite signs.

In order to numerically integrate the cell SPM it is necessary to particularize (8) and (A.1) for the positive and the negative particle and to obtain $C_{sp}(t)$ and $C_{sn}(t)$, respectively, as outputs. Then, these outputs and the cell current $i(t)$ are used in (4) to compute the cell voltage. Next, MATLAB[®]/Simulink[®] software environment is used whenever SPM given by (8) should be run in the different steps of model calibration and validation.

3. SYSTEMATIC METHOD OF SPM CALIBRATION

3.1 Adopted assumptions and methodology

It is well known that precise values of SPM-related parameters are very difficult, if not impossible to obtain. However, variation domains of some of them are known. Thus, values of some of the parameters found in the literature and likely to apply to our modeling problem are taken as a departure point of the proposed calibration method:

- Li^+ concentration in electrolyte phase, C_0 ;
- electrodes' transfer coefficients, α_n and α_p ;
- maximum Li concentrations in solid phase, $C_{m,xn}$ and $C_{m,xp}$;
- volume fractions of solid phase, ϵ_n and ϵ_p ;
- diffusivity coefficient in the solid phase, for the negative particle, D_n (the material is always graphite);
- open-circuit potential for the negative particle as function of lithiation, $U_n(C_{sn})$ (the material is always graphite);
- electrode reaction rates, k_n and k_p .

In a second step, some other material- and geometry-related parameters are measured from the cell itself. This has been done here by using scanning electron microscope, whose results are displayed in Figs. 3 a) and b): electrode area, A ; electrodes' thicknesses L_n and L_p ; radii of positive and negative particles, R_n and R_p , respectively, obtained by averaging grain sizes observed in Figs. 3 a) and b).

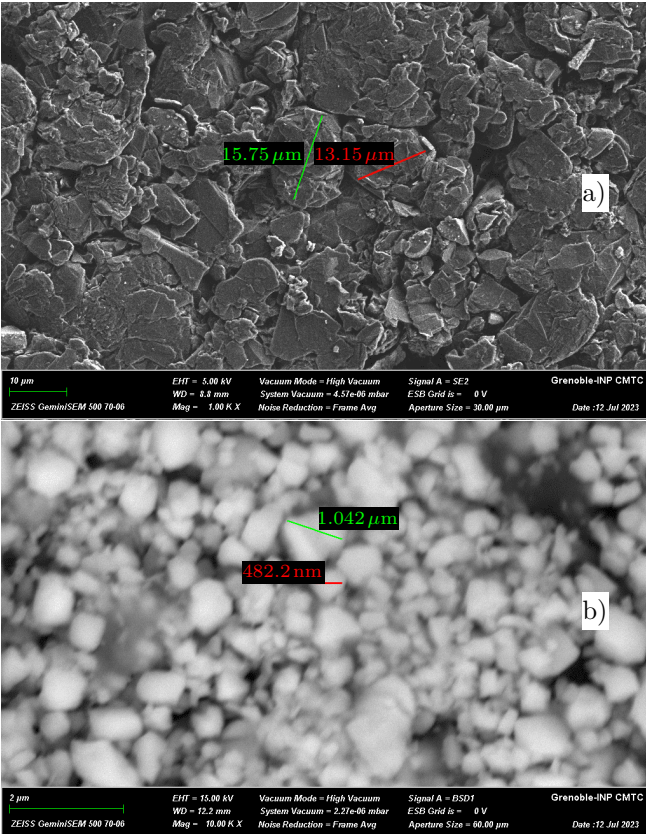


Fig. 3. Measures of the elementary grain radii taken on Panasonic NCR 18650 batteries *via* scanning electron microscopy: a) negative and b) positive electrode.

Electrical measurements were also done. Pseudo-open-circuit voltage for the entire cell as function of SoC, V_{oc} , is obtained from C/20 cell test, involving charging and

discharging at low C-rate. The charge and discharge curves slightly differ, as one obtains a hysteresis-like open-circuit voltage as function of SoC. These are further averaged for each SoC value, to get the function $V_{ocv} = V_{ocv}(\text{SoC})$.

Next, identification aims at separately finding parameters related to open-circuit potentials, *i.e.*, positive diffusivity, D_p , concentrations C_{p0} , C_{p1} and C_{n0} , C_{n1} and the one related to overpotentials, *i.e.*, internal resistance, R_f , by using cell measurements provided by some standard battery cyclers – here, BCS-800-series battery cycler BioLogic (2023) was employed. The influence of the overvoltage component, $V_{out}(t)$, is eliminated during cell relaxation, because the cell current is zero.

3.2 Parameters related to open-circuit potentials

Step 1. Initial data is composed of open-circuit potential, U_n , and the initial value of C_{n1} , which has an educated guess value from the literature. Because the concentration excursion – which is suggested by the red thick line in Fig. 2 b) – is constant for the negative particle, as it depends on known parameters, then only a certain part of curve $U_n(C_{sn})$ is selected.

Step 2. Next, the open-circuit voltage for the entire cell as function of SoC, V_{ocv} , is measured experimentally, by means of C/20 cell test. The open circuit potential for the positive particle, $U_p(C_{sp})$, is obtained by adding the open-circuit potential, $U_n(C_{sn})$, to the open-circuit voltage, V_{ocv} , for the considered lithiation level range.

Step 3. The fully-charged cell is discharged at a constant current during sufficiently long time such that to allow for cell full polarization, then the current is cut off. The relaxation process, which can take as long as 1.5–2 h, is recorded, yielding the cell voltage evolution, v_{cell} , until it reaches the equilibrium relaxation voltage, v_{eq} . Then, the battery voltage variation with respect to measured v_{eq} is obtained: $\Delta v_{cell} = v_{cell} - v_{eq}$.

Step 4. Then, an initial value, corresponding to SoC=1, for the Li concentration in the positive particle, C_{p1} , is chosen and the SPM simulator for the considered cell is run. Two simulations are necessary. The first one aims at obtaining the system state vector when the battery is fully polarized, just before the current is cut off. This is done by running the model simulator from the initial equilibrium state, with constant negative cell current, $i(t) = -I$. Next, cell relaxation is simulated in a second simulation run, starting from the system state vector previously obtained, with zero as input current, for the same time range as in the experiment. The model-computed version of Δv_{cell} , noted as Δv_{bt} , is thus obtained (see Fig. 5).

Step 5. Next, an iterative procedure is initiated, which implements tuning of D_p parameter, such as to minimize the norm of error between Δv_{cell} and Δv_{bt} in the least-squares sense. At the end of the above steps, diffusivity of positive particle, D_p , is obtained.

Step 6. Then, a full discharge at $-1.25C$ (the upper current limit of SPM validity), starting from SoC=1, is simulated. It should be checked if C_{sn} remains strictly positive – see typical evolution in Fig. 6 b). If not, C_{n1} value initially taken at *Step 1* is suitably increased, then go to *Step 1*.

Step 7. Next, C_{n0} and C_{p0} result from model simulation at the previous step, by using current gains G_{in} and G_{ip} and initial respective concentrations at SoC=1; they

are further used as initial concentrations for a simulation consisting of a full charge at +1.25C, starting from SoC=0. It should be checked if C_{sp} remains strictly inferior to C_{maxp} – see typical evolution in Fig. 6 a). If not, C_{p1} value initially taken at *Step 4* is suitably decreased, then go to *Step 4*.

The other limitations in *Step 6* and *Step 7* are out of interest. The excursion of C_{sn} beyond C_{n1} is not critical, as in usual cases $C_{n1} \ll C_{maxn}$; also, the excursion of C_{sp} under C_{p1} is not critical, as habitually $C_{p1} \gg C_{minp}$. Variation ranges of concentrations C_{sn} and C_{sp} should be slightly shifted towards the center of the allowed domain (between 0 and C_{maxn} or between 0 and C_{maxp}) to avoid limitations when submitted to high current. This should not significantly affect the shape of overvoltage (6).

Identification of diffusivity coefficient, D_p , can be performed for any SoC value – that is, by initiating relaxation at an arbitrary time of discharging process – to emphasize the possible variation of this parameter with SoC. To this end, the Coulomb counting technique can in a first place provide a sufficiently reliable SoC estimation.

3.3 Identification of lumped internal resistance

This process is based on the observation that in the first moment of relaxation, an instantaneous voltage drop/rise takes place, depending on the current cell sign. This phenomenon is instantaneous and strictly related to the cumulated overvoltage components – see (6). The first two terms can be computed based on (5) and (4) for given surface Li concentrations, provided that all occurring parameters are now known.

As in the previous identification step, one applies a certain discharging current cell in order to reach a desired SoC level. Then, cell current is cut and instantaneous variation of cell voltage at the moment of zeroing the current, V_{ove} , just before the relaxation process, is recorded.

At the next step, SPM is run as in the previous identification procedure, by using the parameters identified so far and an educated guess value of internal resistance, in order to obtain the simulated cell voltage jump, V_{ovm} . An iterative procedure is subsequently initiated, which implements tuning of R_f parameter such as to minimize the norm of error $V_{ove} - V_{ovm}$ in the least-squares sense. At the end of the above steps, internal resistance value, R_f , is obtained. Likewise diffusivity coefficient, identification of internal resistance can be done for different SoC levels.

The flowchart in Fig. 4 synthesizes the calibration steps, where the possibility of parallel execution is suggested and different colors represent the different types of operations: orange for experiments, blue for model simulation and green for off-line iterative tuning.

4. MODEL VALIDATION AGAINST REAL DATA

4.1 SPM simulation at constant current and relaxation

In this paper, a fresh 3.3 Ah Panasonic NCR 18650 Ga NMC cell – see Panasonic (2023) – has been used for SPM key parameters estimation. All tests – C/20, cell relaxation, current interruption – have been done at controlled temperature (25°C), the cell being connected to the BioLogic battery cycler, and data of interest have been collected by using the associated BT-Lab[®] software.

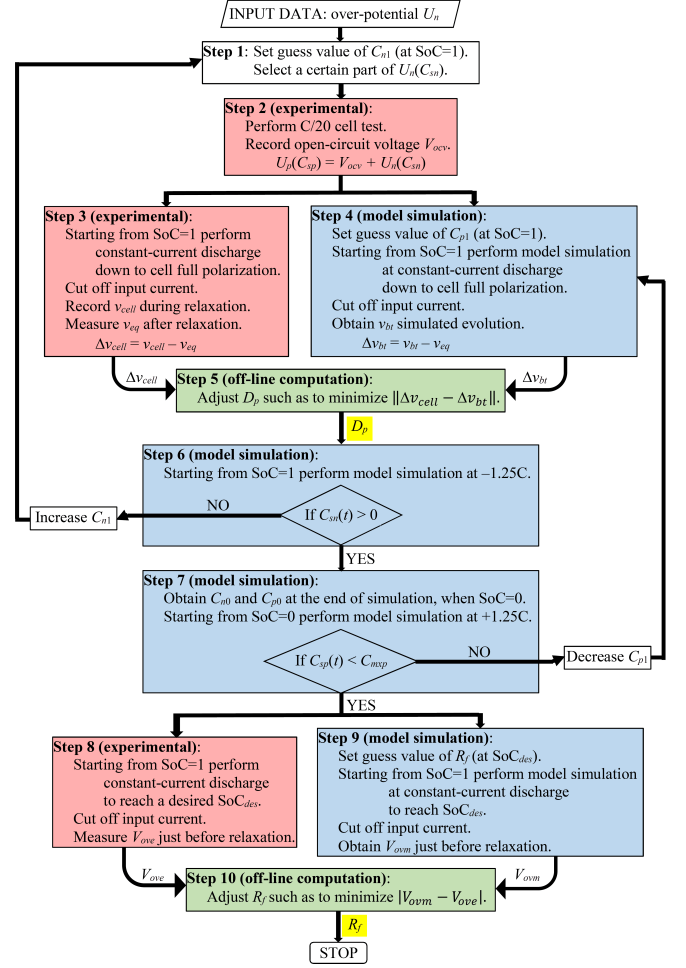


Fig. 4. Calibration algorithm yielding SPM parameters diffusivity coefficient D_p and internal resistance R_f .

Fig. 5 is related to *Steps 1–5* of the algorithm presented in Section 3.2. The blue line represents voltage cell variation, Δv_{cell} , showing cell relaxation towards equilibrium voltage, initial SoC level being 0.8 and the cell being fully polarized. The red line is the output of SPM simulation plotted after the parameter identification. It represents the modeled cell voltage variation, Δv_{bt} , computed for the same initial conditions as the real cell. One can note a close fit between these curves, with a maximum relative error of about 0.15% of the cell rated voltage. Parameters' values used for SPM numerical integration are given in Table A.1 from Appendix A.

Figs. 6 a) – b) concern the *Steps 6–7* of algorithm presented in Section 3.2. They show evolution of Li concentrations for all the $N + 2$ discrete points in the spherical particles while the current is constant, $-1C$, the cell current being further cut off at $t = 3600$ s. One can see the integration effect corresponding physically to Li accumulation and mathematically to the zero eigenvalue of state matrix \mathbf{A}_p in (8). Note the significant dispersion of concentration values, corresponding to cell polarization at constant current, and then the relaxation process, started at $i(t) = 0$, which emphasizes convergence of all concentrations to the unique equilibrium one.

The transient regime differs following the cell current step signs (positive/negative), which may seem weird for a linear system. The relaxation regime at the end of simulation

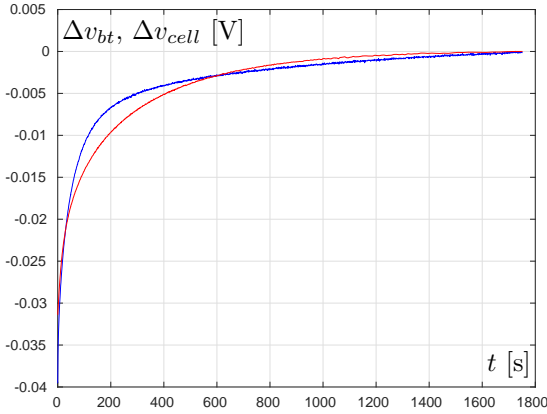


Fig. 5. Voltage cell evolution at relaxation: blue – measured in a dedicated cycler, red – computed *via* model.

lasts significantly longer *vs.* the initial dynamic regime, at the beginning of simulation. This is because the relaxation begins at a moment when the concentration values are dispersed, the system being excited. On the contrary, in the initial regime all the concentrations are equal, the system is initially in equilibrium and the associated dynamic regime lasts significantly shorter.

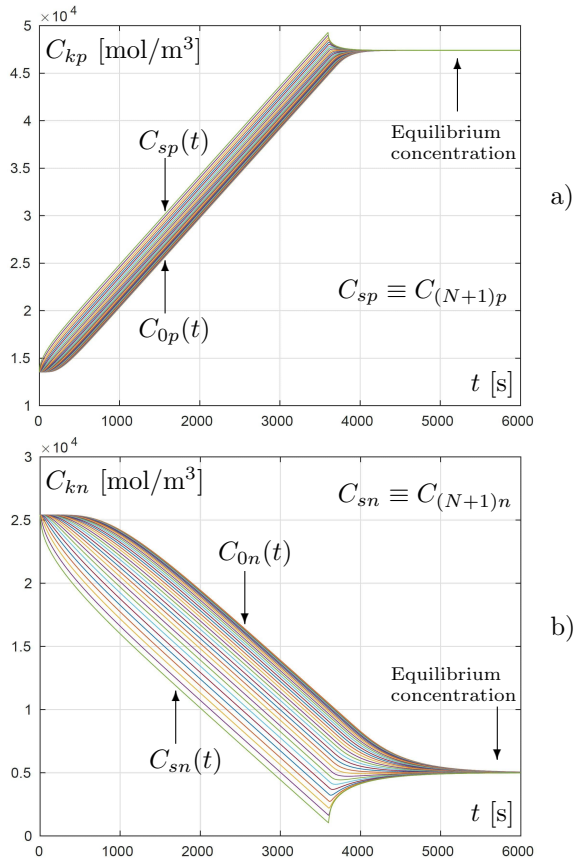


Fig. 6. Discharge at constant current (1C). Evolution of Li concentrations: a) in the positive particle; b) in the negative particle.

4.2 EV-context SPM simulation using identified parameters

A second simulation scenario supposes the application of an EV-specific driving cycle, which here is derived from

the WLTP class 3 current profile – see WLTP3 (2023) and Fig. 7 a). Maximum value in discharge is 1.25C, maximum charging current is 0.55C, average is at 0.15C. This current profile is repeated as long as the cell SoC varies from 1 to 0.2. Fig. 7 b) shows the evolution of simulated cell voltage.

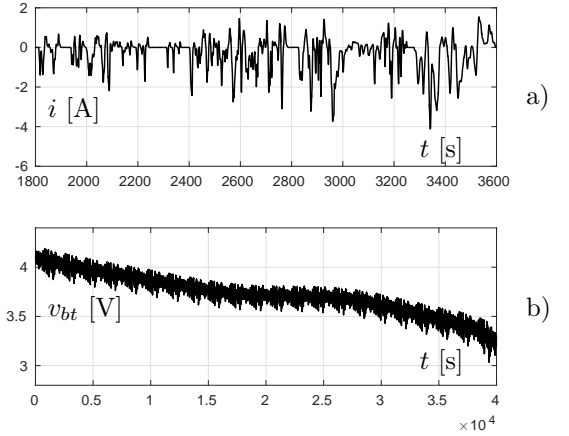


Fig. 7. Discharge with WLTP current profile: a) cell current profile; b) cell voltage evolution.

Fig. 8 shows the SPM-predicted dynamic behavior while submitted to WLTP current profile *vs.* the one of the real cell, in the same conditions, with initial cell SoC around 0.8, *i.e.*, around the identification operation point. A small offset of 0.1 V – *i.e.*, less than 2.5% of the cell rated voltage – amplitude differences around 20 mV and negligible dynamic differences can be noted. However, for some other different SoCs these differences are slightly larger. The offset can be explained by an imprecise identification of the aggregated Li-concentration-variable series resistance corresponding to cell overpotentials (the first two right-side terms of (4) in Section 2). Figs. 9 a) and b) show zooms of Li concentrations' evolutions within the positive and negative particles, in response to the same WLTP current profile. Note that Li concentrations' dispersion within the spheres is larger as the current magnitude is larger.

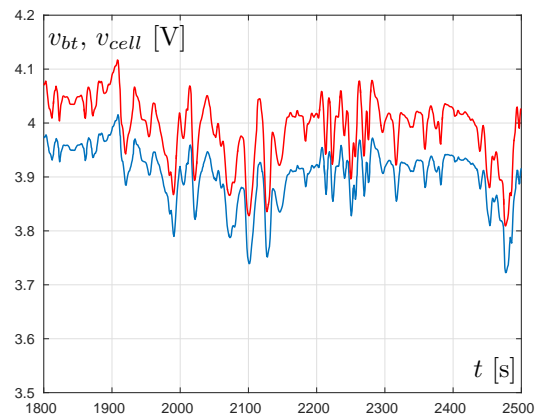


Fig. 8. Voltage behavior in response to WLTP current profile: blue line – cell real data, red line – SPM.

5. CONCLUSION

In this paper, the Single Particle Model (SPM) of Li-ion batteries' internal behavior has been approached as a pertinent solution towards improving estimation accuracy of important characteristics, such as state of charge

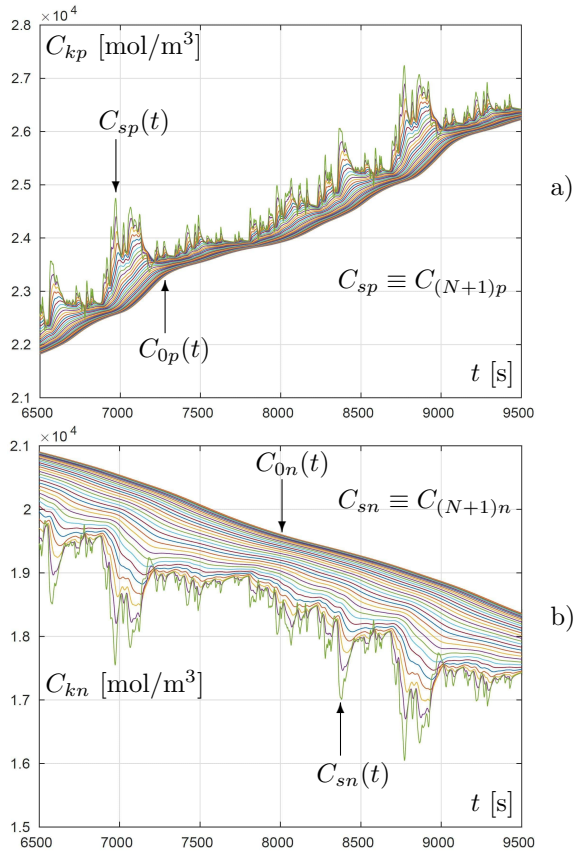


Fig. 9. Discharge with WLTP current profile. Li concentration evolutions: a) in the positive particle; b) in the negative particle.

(SoC) and state of health (SoH), because of its capacity of predicting dynamics of relevant internal variables, such as lithium concentrations within electrodes, and cell voltage response at a certain input current (here, the temperature has been supposed invariant). However, SPM accuracy is counteracted by its complexity, as its numerous parameters are notoriously difficult to measure or estimate.

In SPM each electrode is assimilated to a spherical particle in which spatial Li concentrations evolve according to a diffusion-like process, described by parabolic PDEs. An ODE-based linear dynamic system was obtained as a finite-dimensional approximation, whose states are the volumetric concentrations of Li within the particle (from its center to its surface). Further, the main idea of a SPM-based SoC estimation is that the Li *equilibrium concentration* – obtained as an unique steady-state value of all volumetric concentrations in response to zero cell current, *i.e.*, after the so-called relaxation phase – is an *image of battery* SoC. The equilibrium concentration can easily be computed by the ODE-approximated-SPM numerical integration, provided that all model parameters are either known or properly identified. Thus, a first step of this novel SoC estimation approach has been to propose a systematic, engineering-practice-based method of SPM calibration and validation against real data provided by a dedicated battery cyclers.

An electric vehicular application has been chosen as relevant validation scenario, which has allowed pertinent identification of key parameters. Results suggest good reliability of SPM for estimation of battery various states.

Future work will focus on using previously-calibrated SPM for SoC and SoH estimation, in order to embed them as advanced functions of a battery management system.

REFERENCES

- BioLogic (2023). Biologic ultra-precision battery cyclers. <https://www.biologic.net/products/bcs-800/>. Accessed: April 2024.
- Bizeray, A.M., Kim, J.H., Duncan, S.R., and Howey, D.A. (2018). Identifiability and parameter estimation of the single particle lithium-ion battery model. *IEEE Transactions on Control Systems Technology*, 27(5), 1862–1877.
- Chaturvedi, N.A., Klein, R., Christensen, J., Ahmed, J., and Kojic, A. (2010). Algorithms for advanced battery-management systems. *IEEE Control Systems Magazine*, 30(3), 49–68.
- Di Domenico, D., Stefanopoulou, A., and Fiengo, G. (2010). Lithium-ion battery state of charge and critical surface charge estimation using an electrochemical model-based extended Kalman filter. *Journal of Dynamic Systems, Measurement, and Control*, (132), 1–11.
- Jin, N., Danilov, D.L., Van den Hof, P.M., and Donkers, M. (2018). Parameter estimation of an electrochemistry-based lithium-ion battery model using a two-step procedure and a parameter sensitivity analysis. *International Journal of Energy Research*, 42(7), 2417–2430.
- Klein, R., Chaturvedi, N.A., Christensen, J., Ahmed, J., Findeisen, R., and Kojic, A. (2012). Electrochemical model based observer design for a lithium-ion battery. *IEEE Transactions on Control Systems Technology*, 21(2), 289–301.
- Li, W., Cao, D., Jöst, D., Ringbeck, F., Kuipers, M., Frie, F., and Sauer, D.U. (2020). Parameter sensitivity analysis of electrochemical model-based battery management systems for lithium-ion batteries. *Applied Energy*, 269, 115104.
- Moura, S.J., Argomedeo, F.B., Klein, R., Mirtabatabaei, A., and Krstic, M. (2016). Battery state estimation for a single particle model with electrolyte dynamics. *IEEE Transactions on Control Systems Technology*, 25(2), 453–468.
- Moura, S.J., Krstic, M., and Chaturvedi, N.A. (2012). Adaptive pde observer for battery soc/soh estimation. In *Dynamic Systems and Control Conference*, volume 45295, 101–110. American Society of Mechanical Engineers.
- Panasonic (2023). Ncr18650ga cell datasheet. https://www.omnitron.cz/_dokumenty/792019123600416/ncr-18650ga.pdf. Accessed: April 2024.
- Pozzato, G., Lee, S.B., and Onori, S. (2021). Modeling degradation of lithium-ion batteries for second-life applications: preliminary results. In *2021 IEEE Conference on Control Technology and Applications (CCTA)*, 826–831. IEEE.
- Santhanagopalan, S., Guo, Q., Ramadass, P., and White, R.E. (2006). Review of models for predicting the cycling performance of lithium ion batteries. *Journal of Power Sources*, 156(2), 620–628.
- WLTP3 (2023). Worldwide harmonized light vehicles test cycle. <https://dieselnet.com/standards/cycles/wltp.php#cycles>. Accessed: April 2024.

